RSC Advances

ROYAL SOCIETY OF CHEMISTRY

www.rsc.org/advances

Journal Name

RSCPublishing

COMMUNICATION

Cite this: DOI: 10.1039/x0xx00000x

Nitrogen containing graphene like structures from pyrolysis of pyrimidine polymers for polymer/graphene hybrid field effect transistors

Received ooth January 2012,
Accepted ooth January 2012

DOI: 10.1039/x0xx00000x

www.rsc.org/

Samodha S. Gunathilake, Peishen Huang, Mahesh P. Bhatt, Elizabeth A. Rainbolt

Mihaela C. Stefan*, Michael C. Biewer*[a]

Nitrogen containing graphene like structures were obtained by the pyrolysis of two pyrimidine polymers at 600 °C. Pyrimidine polymers were prepared by the base catalyzed aldol condensation reactions between 2-decyloxy-4,6-dimethylpyrimidine and two aromatic dialdehydes. Pyrolyzed products were shown to have a graphitic structure by Raman spectroscopy, scanning electron microscopy, and powder X-ray diffraction studies. The presence of nitrogen in the graphitic structures was proved by elemental analysis and energy dispersive X-ray analysis experiments. Fluorescence quenching experiments with poly(3-hexylthiophene) (P3HT) showed that the resultant graphitic material can act as acceptor. These materials were tested in P3HT/graphene hybrid field effect transistors which exhibited higher mobilities and comparable on/off ratios compared to P3HT only devices.

Graphene based carbon materials have received a great research focus recently as a material for electronic devices.[1] Graphene is the strongest material ever measured, [2] chemically stable, and conducts electricity better than any previously measured materials at room temperature.[3] However, pure graphene is a zero band gap material, which hinders the use in many electronic devices.[4,5] Therefore, many research efforts are directed towards fine tuning the band gap and thus tailoring the electrical properties of graphene.[5] One of the most feasible methods to tune the band gap of graphene is the chemical modification by doping with heteroatoms.[6] Substitution of some of the carbon atoms in graphene with boron transforms it into a p-type semiconductor, while substitution with nitrogen transforms it into a n-type semiconductor.[7,8] Nitrogen is considered to be an excellent element for chemical doping of graphene because it has comparable atomic size and contains five valence electrons available to form strong valence bonds with carbon atoms.[9] Efforts to introduce nitrogen in graphene structures have included arc discharge method,[10] chemical vapor deposition (CVD) in the presence of ammonia,[11,12] nitrogen plasma treatment of graphene,[13] and CVD with pyridine or other nitrogen containing material.[14] These nitrogen containing graphene materials are promising candidates for a wide range of applications including electrochemical biosensing,[13] lithium ion batteries,[14] fuel cells,[15] solar cells[16,17] and thermoelectric devices.[18]

Another approach for nitrogen doped graphene sheets is by graphitization of a polymer containing nitrogen.[19-22] In this paper we report for the first time the pyrolysis of pyrimidine conjugated polymers to obtain nitrogen containing graphene like structures which were employed in hybrid field effect transistors with poly(3-hexylthiophene) (P3HT). To show the general applicability of pyrimidine conjugated polymers to obtained nitrogen doped graphitic materials two different pyrimidine polymers were employed and they were synthesized by base catalyzed aldol condensation reactions between 2-decyloxy-4,6-dimethylpyrimidine and terephthalaldehyde and isophthalaldehyde, respectively. We reported the synthesis of polymer **P1** in our previous paper.[23]

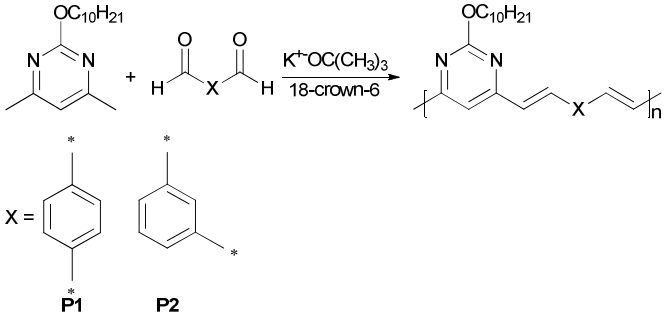

Scheme 1. Synthetic route for pyrimidine polymers

Scheme 1 shows the synthetic route used to synthesize polymers **P1** and **P2**. The synthesized polymers had limited solubility in common organic solvents such as chloroform, chlorobenzene, toluene, and tetrahydrofuran. The soluble fraction was used to characterize the polymers and the insoluble high molecular weight fraction was used for pyrolysis. Polymers were characterized by using ^{1}H-NMR and UV-visible spectroscopy. The molecular weights of the polymers were measured by size exclusion chromatography (SEC). The number average molecular weight (M_n) of **P1** was 7500 g mol^{-1} with a polydispersity index (PDI) of 1.6. Polymer **P2** had a M_n of 5540 g mol^{-1} with a PDI of 2.7. The NMR spectra of monomers, polymers and the UV-visible spectra of polymers in chloroform solution are given in supporting information. UV-visible spectra of polymers **P1** and **P2** in chloroform solution showed one absorption maximum centered at 385 nm and 329 nm for **P1** and **P2**, respectively. This is due to π-π* transition along the backbone of the polymer. Absorption maximum of **P1** was red shifted as compared to **P2** which was attributed to the higher molecular weight of **P1**. Thermogravimetric analysis (TGA) was carried on **P1** and **P2** and both polymers showed thermal stability up to ~300 °C. A 5% weight loss at 334 °C and 310 °C was observed for polymers **P1** and **P2**,

respectively. After studying the thermal stability of polymers, they were pyrolyzed by placing a known amount of the polymer in a vertical silica furnace and raising the temperature to the required temperature under nitrogen. The desired temperature was maintained for 3 hours, after that the samples were cooled down to room temperature under nitrogen. Temperature studies on pyrolysis were carried out by using Raman spectroscopy with excitation laser wavelength of 632 nm. Since polymers are thermally stable up to 300 °C, as determined by TGA analysis, temperature studies were carried out at temperatures above 300 °C. Temperature range studied was 300 °C-600 °C and the resultant Raman spectra were compared to that of original polymers before pyrolysis. Characteristic Raman D(1330 cm^{-1}), G (1580 cm^{-1}) and 2D (2800 cm^{-1}) bands were not observed at temperatures below 450 °C and started to appear at temperatures above 450 °C for both polymers. Polymers before pyrolysis show a broad peak centered around 2800 cm^{-1} as all kinds of sp^2 hybridized carbon materials exhibit. This could also be due to sp^3 C-H stretching in alkoxy substituents attached the polymer backbone. We speculate that due to the high temperature treatment these alkoxy groups were removed, therefore, as the temperature increased, the intensity of 2D peak decreased. When the temperature is increased above 450 °, this peak is associated with D and G bands and is called 2D band. [24,25] Raman spectra at different temperatures for polymer **P1** are shown in figure 1.

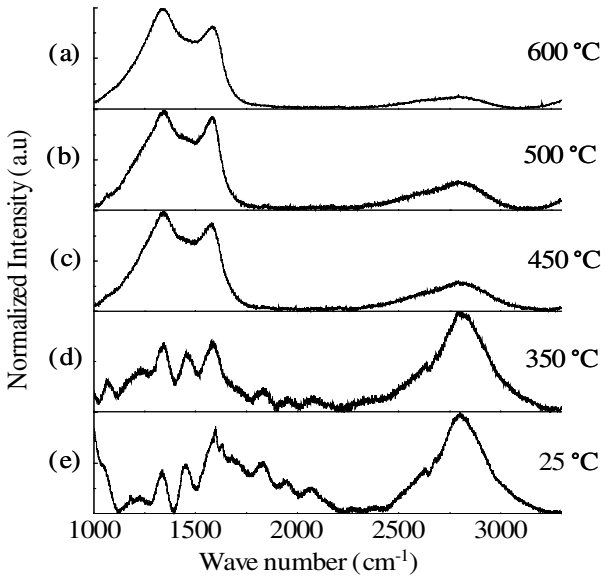

Figure 1. Raman spectra at (a) 600 °C, (b) 500 °C, (c) 450 °C, (d) 350 °C and (e) room temperature (25 °C) for **P1**

Polymer **P2** showed the same behavior and the Raman spectra are given in supporting information. The intensity of the D band of these Raman spectra is high compared to G band, possibly due to the introduction of nitrogen. This suggests the doped nitrogen could be either pyrrolic or pyridinic. Further 2D band of these Raman spectra are broad, could be due to the strain induced by the high temperature treatment during pyrolysis process.[27] The 2D band of graphitic materials is sensitive to temperature and upon increasing the temperature, the intensity of 2D peak decreases because of the doping effect induced by temperature. [28] Pyrolyzed product from **P1** at 600 °C for 3 hours (**G1**) and pyrolyzed product from **P2** at 600 °C for 3 hours (**G2**) were used for further characterizations and fabrication of hybrid field effect transistors.

Powder X-ray diffraction measurements were conducted for polymers **P1** and **P2** and for the graphitized materials **G1** and **G2** on Rigaku Ultima IV X-ray diffractometer with Cu-Kα radiation and scan rate of 1 degree/min. Broad peaks at 2θ = 19.9° for **P1** and 2θ = 20.5° for **P2** correspond to d-spacings of 4.45 Å and 4.32 Å respectively. These halo-like broad peaks indicate that **P1** and **P2** are amorphous.[26] Upon pyrolysis these broad peaks were shifted to higher 2θ values with 2θ= 24.0° for **G1** and 2θ = 23.7° for **G2**. These are corresponding to d-spacings of 3.70 Å for **G1** and 3.74 Å for **G2**. The calculated d-spacing values strongly suggest a 2-D layering similar to graphene sheets. The formation of graphene sheets was further proved by scanning electron microscopy (SEM) analysis performed with a Zeiss-LEO model 1530 SEM instrument. Transformation from granular morphology of **P1** and **P2** to layered morphology of **G1** and **G2** clearly showed the layer formation as shown in figure 2. The estimated layer thickness from the SEM images was ~ 28 nm.

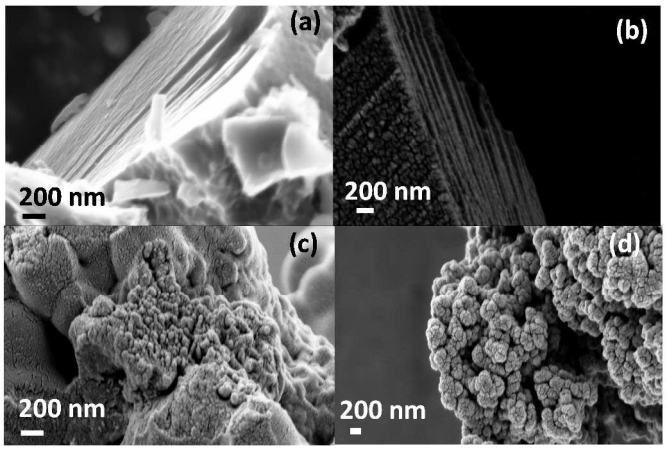

Figure 2. SEM of (a) **G1**, (b) **G2**, (c) **P1** and (d) **P2**.

Electron accepting behavior of **G1** and **G2** was studied by fluorescence quenching experiments on Perkin–Elmer LS50 BL luminescence spectrometer with p-type polymer poly(3-hexylthiophene) (P3HT) (M_n = 51840 g mol^{-1}, PDI = 2.1). Solution of P3HT in chlorobenzene was prepared with a concentration of 0.01 mg/mL and **G1** (or **G2**) was dispersed in polymer solution by varying P3HT/**G1** (or **G2**) weight ratios ranging from 1:5 to 1:45. A control solution was prepared by dispersing **G1** (or **G2**) in chlorobenzene with a concentration of 1 mg/mL. Excitation wavelength was determined to be 458 nm from UV-visible spectroscopy. Emission peak was obtained at 575 nm and as can be seen from figure 3 the intensity of emission peak decreased as the amount of **G1** (or **G2**) increased and no emission peak was observed for the control experiment at the same excitation wavelength. These results indicate that **G1** and **G2** behave as electron accepting materials.

The presence of nitrogen in the pyrolyzed products was confirmed by energy dispersive X-ray (EDS) experiments qualitatively and by elemental analysis by combustion method quantitatively. In EDS spectrum peak for carbon Kα at 0.2774 eV and peak for nitrogen Kα at 0.3924 eV are overlapping as shown in figure 4(b) and elemental mapping for carbon and nitrogen is shown in figure 4(c) and 4(d). Pyrolyzed product **G2** showed similar results (supporting information).

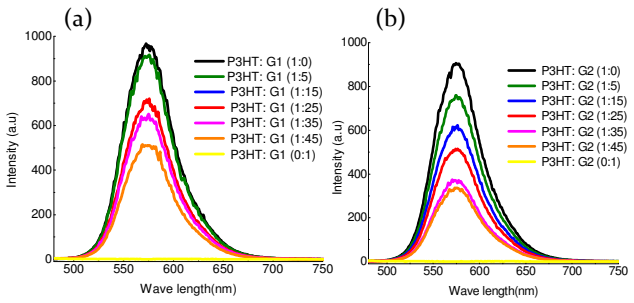

Figure 3. Fluoresence quenching of P3HT with **G1** (a), **G2** (b)

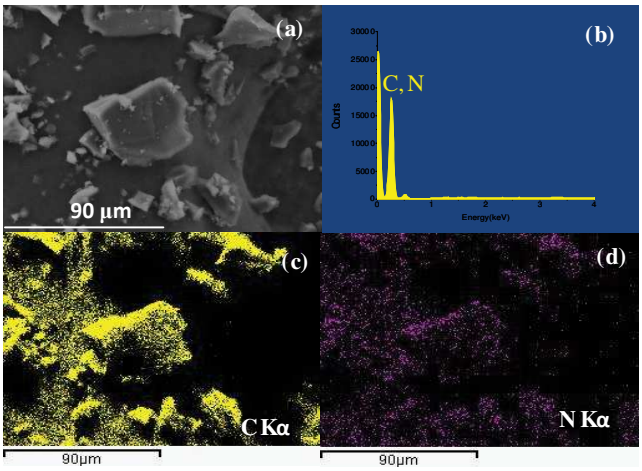

Figure 4. SEM of **G2** where EDS was performed (a), EDS spectrum (b), Elemental mapping for carbon (c) and elemental mapping for nitrogen (d).

According to the elemental analysis by combustion method, **G1** contained ~6.98 % nitrogen which is slightly larger than that of **G2** which contained ~6.10 % nitrogen.

The use of this nitrogen containing graphene like materials in polymer/graphene hybrid field effect transistors resulted in increase in mobility and comparable on/off ratios compared to control P3HT field effect transistors. Polymer/graphene hybrid field effect transistor devices offer advantageous characteristics from both polymer and graphene, that is, high conductivity of graphene and solution processability and flexibility of polymers. To investigate the effect of polymer molecular weight on the hybrid field effect transistor performance, P3HT with two different molecular weights were employed. One set of hybrid field effect transistor devices were prepared by using P3HT with M_n = 51840 g mol^{-1}, PDI = 2.1 and the second set was prepared by using P3HT with M_n = 13600 g mol^{-1}, PDI = 1.3. Concentration of P3HT was kept constant at 1 mg/mL for both P3HT and P3HT/**G1** (or **G2**) blend solutions. **G1** (or **G2**) dispersions were prepared by solution sonication method. Briefly, **G1** (or **G2**) (10 mg) was added to chlorobenzene (2 mL) for a concentration of 5 mg/mL. The mixture was sonicated for two hours. After sonication, dispersions were left to stand for 1 hour to allow the large particles to settle down. Top portion of the dispersion was separated from the large particles settled at the bottom of the vial. The concentration of **G1** (or **G2**) in dispersions were measured by adding a known volume of the dispersion onto a heated glass substrate. After the complete solvent evaporation mass change was obtained and the concentration was calculated to be 1 mg/mL. To make P3HT/**G1** (or **G2**) composites, 1 mg of P3HT was dissolved in 1 mL of the resultant **G1** (or **G2**) dispersion. The mixture was heated to allow the polymer to dissolve completely and cooled down to room temperature before depositing on the field effect transistor devices. P3HT/**G1** (or **G2**) composites had a dark brown color compared to orange color of P3HT solution. Field effect transistor device measurements were performed using bottom gate bottom contact device configuration.

Highly doped, n-type silicon wafers with a resistivity of 0.001–0.003 Ω cm were used as substrates. Thermal oxide (SiO_2) was thermally grown at 1000 °C on silicon substrate to obtain a 200 nm thickness. Chromium metal (5 nm) followed by 100 nm of gold was deposited by E-beam evaporation as source-drain contacts. The source-drain pads were made by photolithographically patterning the metal layer. The SiO_2 on the back side of the wafer was etched with buffered oxide etchant (BOE from JT Baker) to generate the bottom-gate. The resulting transistors had a channel width of 475 µm and channel lengths varying from 2 to 80 µm. The measured capacitance density of the SiO_2 dielectric was 17 nF/cm^2. Before deposition of the samples, the substrates were cleaned by UV/ozone for 10 minutes. The devices were then rinsed in air with water, methanol, hexane, chloroform, and dried with nitrogen flow followed by vacuum for 30 minutes at 80 °C.

Hybrid field effect transistors were fabricated by drop casting P3HT/**G1** (or **G2**) composite solutions on heated substrate at 40 °C. Control devices were fabricated by using the same procedure with pure P3HT in chlorobenzene. The devices were annealed at 120 °C for 30 minutes before taking measurements. Transfer characteristics and output characteristics of the hybrid field effect transistors and controlled polymer field effects transistors with P3HT of M_n = 51840 g mol^{-1}, PDI = 2.1 are shown in figure 5. The corresponding plots for the hybrid field effect transistors with P3HT of M_n = 13600 g mol^{-1}, PDI = 1.3 are given in supporting information.

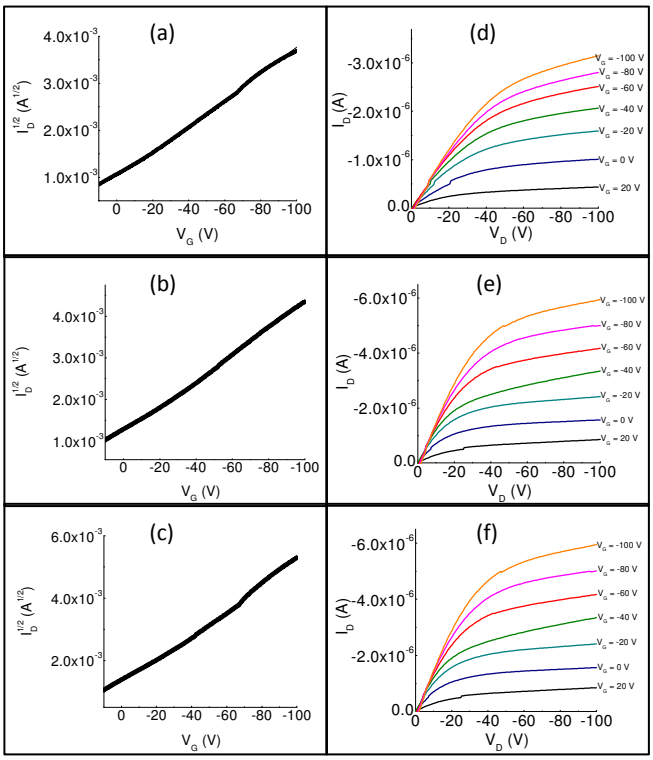

Figure 5. (Left) Transfer characteristics of FETs (a) P3HT, (b) P3HT/**G1**, (c) P3HT/**G2**, (right) output characteristics of FETs (d) P3HT, (e) P3HT/**G1** and (f) P3HT/**G2** with P3HT of M_n = 51840 g mol^{-1}, PDI = 2.1

Table 1 summarizes the mobility and on/off ratios of the hybrid devices and control devices. Compared to control P3HT field effect transistor devices, P3HT/**G1** and P3HT/**G2** hybrid field effect devices show higher mobilities and similar on/off ratios in both cases. These values are from the measurements performed in ambient air and the on/off ratio can improve if the measurements are performed under nitrogen. Higher mobility of hybrid devices compared to control devices can be explained as graphitic structures **G1** and **G2** provide a good connectivity between the crystalline domains of P3HT film.[29] This was further confirmed by tapping mode atomic force microscopy (TMAFM) analysis which was performed on channel region of the field effect transistor devices. The surface roughness of the P3HT/**G1** and PHT/**G2** composites increased as compared to the control P3HT devices (table 1 and figure 6). A granular morphology was observed for both P3HT and P3HT graphene devices. Granular morphologies for P3HT devices have been shown to give relatively high mobilities.[30] The observed increase in surface roughness (rms) (table 1) for the hybrid devices could indicate larger granular domains which in turn resulted in less grain boundaries between adjacent nanofibers of P3HT to obtain increased mobility for the hybrid devices as compared to P3HT. Our data are consistent with previous report in which it was shown that the grain boundaries between polycrystalline domains of P3HT resulted in increased resistance for charge carriers which in turn gave lower mobilities.[31-33] Further the high charge carrier mobility of hybrid devices compared to control devices can be also due to the doping of P3HT by n-type nitrogen doped **G1** and **G2**. These nitrogen doped **G1** and **G2** can partially oxidized P3HT to give high charge carrier mobilities. Threshold voltages of the devices were relatively high which could be due to the doping effect induced by air (all the OFET measurements were carried out in ambient air).

Table 1. Mobility and on/off ratio for control and hybrid field effect transistor devices

	Material	Mobility ($cm^2V^{-1}S^{-1}$)		On/off ratio	rms[c]
		Average	Maximum		
(1)[a]	P3HT	3.3×10^{-3}	3.9×10^{-3}	10^2	4.0
	P3HT/G1	2.5×10^{-2}	5.4×10^{-2}	10^2	4.3
	P3HT/G2	1.1×10^{-2}	1.4×10^{-2}	10^2	4.9
(2)[b]	P3HT	4.35×10^{-4}	5.48×10^{-4}	10^1	1.9
	P3HT/G1	1.02×10^{-3}	1.34×10^{-3}	10^1	2.2
	P3HT/G2	1.14×10^{-3}	1.56×10^{-3}	10^1	2.3

[a] P3HT with 51840 g mol^{-1}, PDI = 2.1, [b] P3HT with 13600 g mol^{-1}, PDI = 1.3, [c] Root mean square roughness of thin films

The XRD analysis showed that the d-spacing of second order diffractions of P3HT were slightly decreased in the P3HT/**G1** (or **G2**) blends. Especially the diffraction peak at 16.0 ° for P3HT has been shifted to higher 2θ value in both composites. Largest shift was observed for high molecular weight P3HT/**G1** composite, which also showed the highest increase in mobility. The intensity of second order diffractions and π-π stacking peaks were decreased in P3HT/**G1** (or **G2**) blends as compared to that of the polymers. This could be interpreted as indicative of formation of larger granular domains of P3HT that were also suggested by the TMAFM studies. (The XRD patterns and calculated d-spacing values are given in supporting information)

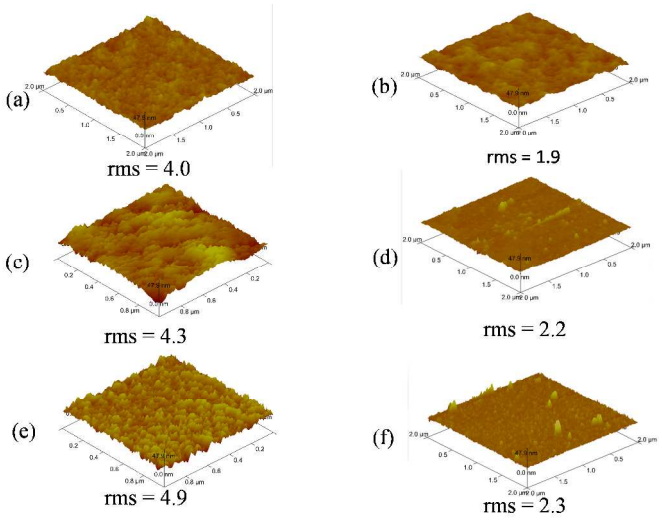

Figure 6: 3D TMAFM images of the channel region in FET devices (a) P3HT (M_n = 51840 g mol^{-1}), (b) P3HT (M_n = 13600 g mol^{-1}), (c) P3HT/**G1**(M_n = 51840 g mol^{-1}), (d) P3HT/**G1** (M_n = 13600 g mol^{-1}), (e) P3HT/**G2** (M_n = 51840 g mol^{-1}), (f)) P3HT/**G2** (M_n = 13600 g mol^{-1}).

Conclusions

In conclusion, nitrogen doped graphene like structures were obtained by pyrolysis of pyrimidine conjugated polymers synthesized through base catalyzed aldol condensation reactions. The graphitized products contained ~ 7% nitrogen. These graphene-like materials increased the mobility of polymer/graphene hybrid field effect transistors. These results show that pyrimidine polymers are a good source to generate nitrogen doped graphene materials. The structures of pyrimidine conjugated polymers can be further tuned to obtain more ordered graphene materials which are expected to generate improved optoelectronic properties. In addition, this method can be tailored to create graphene-like materials with a systematic control of nitrogen content within the graphitized structure.

Notes and references

[a]University of Texas at Dallas, Department of Chemistry, 800 West Campbell Road, Richardson, TX 75080, USA. Financial support for this project from NSF (Career DMR-0956116) and Welch Foundation (AT-1740) is gratefully acknowledged. We gratefully acknowledge the NSF-MRI grant (CHE-1126177) used to purchase the Bruker Avance III 500 NMR instrument.

1. K. S. Novoselov, A. K. Geim, S. V. Morozov, D. Jiang, Y. Zhang, S. V. Dubonos, I. V. Grigorieva, A. A. Firsov, *Science,* 2004, **306**, 666.

2. C. Lee, X. Wei, J. W. Kysar, J. Hone, *Science,* 2008, **321**, 385.

3. L. A. Ponomarenko, F. Schedin, M. I. Katsnelson, R. Yang, E. W Hill, K. S. Novoselov, K. Geim, *Science,* 2008, **320**, 356.

4. Q. Tang, Z. Zhou, Z. Chen, *Nanoscale,* 2013, **5**, 4541.

5. D. Usachov, O. Vilkov, A. Gruneis, D. Haberer, A. Federov, V. K. Adamchuk, A. B. Preobrajenski, P. Dubin, A. Barinov, M. Oehzelt, C. Laubschat, D. V. Vyalikh, *Nano Lett,*. 2011, **11**, 5401.

6. H. Liu, Y. Liu, D. Zhu, *J. Mater. Chem.,* 2011, **21**, 3335.

7. L. Zhao, R. He, K. T. Rim, T. Schiros, K. S. Kim, H. Zhou, C. Gutierrez, S. P. Chockalingam, C. J. Arguello, L. Palova, D. Nordlund, M. S. Hybertsen, D. R. Reichman, T. F. Heinz, P. Kim, A. Pinczuk, G. W. Flynn, A. N. Pasupathy, *Science,* 2011, **333**, 999.

8. A. Lherbier, X. Blasé, Y. M. Niquet, F. Triozon, S. Roche, *Phys. Rev. Lett,.* 2008, **101**, 036808.

9. S. U. Lee, R. V. Belosludov, *Small,* 2009, **5**, 1769.

10. L.S. Panchokarla, K. S. Subrahmanyam, K. S. Saha, A. Govindaraj, H. R. Krishnamurthy, U. V. Waghmare, C. N. R. Rao, *Adv. Mater.,* 2009, **21**, 4726.

11. C. D. Wei, Y. Q. Liu, W. Wang, H. L. Zhang, L. P. Huang, G. Yu, *Nano Lett.,* 2009, **9**, 1752.

12. L. Qu, Y. Liu, J. B. Beak, L. Dai, *ACS Nano,* 2010, **4**, 1321.

13. Y. Wang, Y. Shao, D. W. Matson, J. Li, Y. Lin, *ACS Nano,* 2010, **4**, 1790.

14. Z. Jin, J. Yao, C. Kittrell, J. M. Tour, *ACS Nano,* 2011, **5**, 4112.

15. A. L. M. Reddy, A. Srivastava, S. R. Gowda, H. Gullapalli, M. Dubey, P. M. Ajayan, *ACS Nano,* 2010, **4**, 6337.

16. X. Wang, L. J. Zhi, K. Mullen, *Nano Lett.,* 2008, **8**, 323.

17. H. Ming, J. Jaehan, Q. Feng, L. Zhiqun, *J. Mater. Chem.,* 2012, **22,** 24254.

18. M. He, F. Qiu, Z. Lin, *Energy Environ. Sci.,* 2013, **6,** 1352.

19. M. C. Suh, S. C. Shim, *Chem Mater,* 1997, **9**, 192.

20. H. Konno, T. Nakahashi, M. Inagaki, *Carbon,* 1997, **5**, 669.

21. Z. Sun, Z. Yan, J. Yao, E. Beitler, Y. Zhu, J. M. Tour, *Nature,* 2010, **468,** 549.

22. S. J. Byun, H. Lim, G. Y. Shin, T. H. Han, S. H. Oh, J. H. Ahn, H. C. Choi, T. W. Lee, *J. Phys. Chem.,Lett.,* 2011, **2,** 493.

23. S. S. Gunathilake,H. D. Magurudeniya, P. Huang, H. Nguyen, E. Rainbolt, M. C. Stefan, M. C. Biewer, *Polym. Chem.,* 2013, **4**, 5216.

24. M. S. Dresselhaus, A. Jori, M. Hofmann, G. Dresselhaus, R. Saito, *Nano Lett.* 2010**, 10,** 751

25. A. C. Ferrari, J. Robertson, *Phys. Rev. B,* 2001, **64,** 075414

26. H. Kong, D. H. Lee, J. I. Seo, J. Y. Oh, D. S. Chung, J. W. Park, S. K. Kwon, Y. S. Lee, C. E. Park, H. K. Shim, ACS: *Appl. Mater. and Interfaces,* 2010, **4**, 1100.

27. M. Xia, Z. Su, S. Zhang, *AIP Advances,* 2012, **2,** 032122.

28. L. M. Malard, R. L. Moreira, D. C. Elias, F. Plentz, E. S. Alves, M. A. Pimenta, *J. Phys. :Condens. Mater,* **22,** 2010, 334202.

29. J. Huang, D. R. Hines, B. J. Jung, M. S. Bronsgeest, A. Tunnell, V. Ballarotto, H. E. Katz, M. S. Fuhrer, E. D. Williams, J. Cumings, *Org. Electro.,* 2011, **12,** 147.

30. T. L. Nelson, T. M. Young, J. L. Sarada, P. Mishra, J. A. Belot, C. L. Balliet, A. E. Javier, T. Kowalewski, R. D. McCullough, *Adv. Mater.,* 2010, **22,** 4617.

31. R. Zhang, B. Li, M. C. Iovu, M. Jeffries-EL, G. Sauve, J. Cooper, S. Jia, S. T. Nagle, D. M. Smilgies, D. N. Lambeth, R. D. McCullough, T. Kowalewski, *J. Am. Chem. Soc.,* 2006, **128,** 3480.

32. H. Meng, J. Zheng, A. J. Lovinger, B. C. Wang, P. G. V. Patten, Z. Bao, *Chem Mater.,* 2013, **15,** 1778.

33. H. Yang, T. J. Shin, L. Yang, K. Cho, C. Y. Ryu, Z. Bao, *Adv. Funct. Mater.,* 2005, **15,** 671.